

AD-A247 546



PL-TR-91-2250

E 200 901

(2)

THE DISTANCE DEPENDENCE OF REGIONAL PHASE DISCRIMINANTS

Brian L. N. Kennett

Australian National University
Research School of Earth Sciences
GPO Box 4
Canberra ACT 2601
AUSTRALIA

4 October 1991

Scientific Report No. 1



APPROVED FOR PUBLIC RELEASE; DISTRIBUTION UNLIMITED



PHILLIPS LABORATORY
AIR FORCE SYSTEMS COMMAND
HANSOM AIR FORCE BASE, MASSACHUSETTS 01731-5000

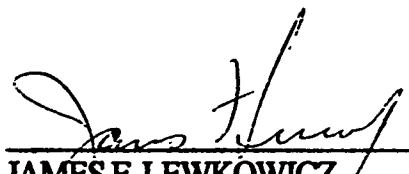
92 2 18 184

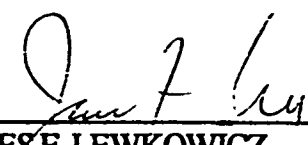
92-04154



The views and conclusions contained in this document are those of the authors and should not be interpreted as representing the official policies, either expressed or implied, of the Air Force or the U.S. Government.

This technical report has been reviewed and is approved for publication.


JAMES F. LEWKOWICZ
Contract Manager
Solid Earth Geophysics Branch
Earth Sciences Division


JAMES F. LEWKOWICZ
Branch Chief
Solid Earth Geophysics Branch
Earth Sciences Division


DONALD H. ECKHARDT, Director
Earth Sciences Division

This document has been reviewed by the ESD Public Affairs Office (PA) and is releasable to the National Technical Information Service (NTIS).

Qualified requestors may obtain additional copies from the Defense Technical Information Center. All others should apply to the National Technical Information Service.

If your address has changed, or if you wish to be removed from the mailing list, or if the addressee is no longer employed by your organization, please notify PL/IMA, Hanscom AFB MA 01731-5000. This will assist us in maintaining a current mailing list.

Do not return copies of this report unless contractual obligations or notices on a specific document requires that it be returned.

REPORT DOCUMENTATION PAGE			Form Approved OMB No. 0704-0188	
<small>1. The reporting burden for this collection of information is estimated to average 1 hour per response, including the time for reviewing instructions, searching existing data sources, gathering and maintaining the data needed, completing and reviewing the collection of information, sending comments regarding this burden estimate or any other aspect of this collection of information, including suggestions for reducing this burden to Washington Headquarters Services, Directorate for Information Operations and Reports, 1215 Jefferson Davis Highway, Suite 1204, Arlington, VA 22202-4302, and to the Office of Management and Budget, Paperwork Reduction Project (0704-0188), Washington, DC 20503.</small>				
1. AGENCY USE ONLY (Leave blank)		2. REPORT DATE 4 October 1991	3. REPORT TYPE AND DATES COVERED Scientific #1 (30 Sept 1990-29 Sept 1991)	
4. TITLE AND SUBTITLE The Distance Dependence of Regional Phase Discriminants			5. FUNDING NUMBERS Contract APOSR-90-0352	
6. AUTHOR(S) Brian L.N. Kennett			PE: 62101F PR 7600 TA 09 WU AO	
7. PERFORMING ORGANIZATION NAME(S) AND ADDRESS(ES) Australian National University Research School of Earth Sciences GPO Box 4 CANBERRA ACT 2601 Australia			8. PERFORMING ORGANIZATION REPORT NUMBER	
9. SPONSORING/MONITORING AGENCY NAME(S) AND ADDRESS(ES) Phillips Laboratory Wanskam AFB, MA 01731-500 Contract Manager: James Lewkowicz/LWH			10. SPONSORING/MONITORING AGENCY REPORT NUMBER PL-TR-91-2250	
11. SUPPLEMENTARY NOTES				
12a. DISTRIBUTION/AVAILABILITY STATEMENT APPROVED FOR PUBLIC RELEASE: DISTRIBUTION UNLIMITED			12b. DISTRIBUTION CODE	
13. ABSTRACT (Maximum 200 words) A number of proposed discriminants for distinguishing the character of seismic sources use the amplitude of the phase Pn as a reference. The merit of Pn is that it constitutes the onset of regional seismograms, but the behaviour of the arrivals at an individual station can be quite complex. Results from long-range refraction experiments in Eurasia suggest that the complexity arises from the superposition of a number of sub-phases returned from fine-scale structure in the uppermost mantle. The behaviour is consistent with fine scale horizontal variations superimposed on a gentle increase in seismic velocity with depth, so that equivalent one-dimensional models will show multiple low velocity zones. Long range refraction data for Sn is much less common but similar trends can be discerned. As frequency increases such complexity is likely to become more important. Sn is often observed at distance beyond 300 km but emerges from Sg(Lg) much less clearly in general than Pn emerges from Pg. However some refraction profiles in the Finnish Shield areas show very clear Sn arrivals at short distances. The differences in character can be associated with differing velocity gradients for S in the uppermost mantle. The variability in Sn behaviour means that it may prove difficult to generate discriminants based on e.g. Pn/Sn amplitude which can be readily transportable between different regions.				
14. SUBJECT TERMS Wave Propagation, Regional Phases, Pn, Sn, Refraction Studies, Heterogeneity			15. NUMBER OF PAGES 38	
			16. PRICE CODE	
17. SECURITY CLASSIFICATION OF REPORT Unclassified	18. SECURITY CLASSIFICATION OF THIS PAGE Unclassified	19. SECURITY CLASSIFICATION OF ABSTRACT Unclassified	20. LIMITATION OF ABSTRACT SAR	

CONTENTS

INTRODUCTION	1
THE PHYSICAL CHARACTER OF REGIONAL PHASES	1
OBSERVATIONS OF MANTLE PHASES	6
THEORETICAL STUDIES	17
CONCLUSIONS	21
REFERENCES	24



Accession For	
NTIS GRA&I	<input checked="" type="checkbox"/>
DTIC TAB	<input type="checkbox"/>
Unannounced	<input type="checkbox"/>
Justification	
By _____	
Distribution/	
Availability Codes	
Dist	Avail and/or Special
A-1	

Figure 1: A schematic representation of the propagation processes which need to be included in the description of mantle phases (after Kennett 1989b).

Figure 2: Script file display for the adaptation of the iasp91 travel time routines to display phase and group velocities in order to compare the ray based assignments of conventional location procedures with the discrimination phases Pg, Lg.

Figure 3: WKBJ synthetic seismogram for a simple crustal model representative of a shield region. Up to 4 crustal multiples are allowed for reflection from each interface or for diving waves. The P and S wave calculations were carried out separately and superimposed in plotting.

Figure 4: Recordings of an earthquake (FF) and a quarry blast (SM) along the same array of portable seismographs in southeastern Australia. In each case the Pn phase can be clearly observed even though the earthquake phase are close to a node for P, it is much more difficult to detect the Sn arrival even with a number of records.

Figure 5: P and S wave sections for the vertical component of displacement for an earthquake in northwestern Scotland recorded during the long-range refraction profile through the British Isles. The reduction velocity for the P section is 8 km/s, and for the S section it is 4.62 km/s (after Kaminiski et al 1974).

Figure 6: Three component record sections for a large explosive shot off the French coast recorded across a long range profile in France (after Hirn 1977). Reduction velocity for the Z section is 8 km/s, whereas for the L and T sections the velocity is 4.62 km/s

Figure 7: Ray diagram illustrating the way in which a mantle structure with a number of gradient zones can give rise to a sequence of phases returned from the mantle with an apparent en-echelon behaviour in time.

Figure 8: Configuration of the SVEKA and BALTIC and POLAR refraction experiments in Fennoscandia.

Figure 9: Comparison of P and S record sections from the SVEKA refraction profile in Finland using vertical component seismometers, the traces are amplitude normalised. The reduction velocity for the P section is 8 km/s, and for the S section it is 4.62 km/s (after Luosto et al 1984, Grad & Luosto 1987).

Figure 10: Comparison of P and S record sections from the BALTIC refraction profile in Finland using vertical component seismometers, the traces are amplitude normalised. The reduction velocity for the P section is 8 km/s, and for the S section it is 4.62 km/s

Figure 11: Comparison of P and S record sections from the POLAR refraction profile in northern Fennoscandia using vertical component seismometers, the traces are amplitude normalised. The reduction velocity for the P section is 8 km/s, and for the S section 4.62 km/s (after Luosto et al 1989).

Figure 12: Portion of a record section assembled from hand-digitised seismograms from a detailed DSS profile across the southern Ukrainian shield with reduction velocity 6 km/s. The amplitude variability across the very close trace spacing (around 200 m) illustrates the problems involved in trying to use the ratios of different seismic phases as measures of source radiation patterns (after Jentsch 1979).

Figure 13: Portion of the record section from a DSS profile in northern Siberia, the reduction velocity is 8.2 km/s (after Yegorkin & Chernyshov 1983).

Figure 14: Amplitude distance behaviour for topography at the crust-mantle boundary. Solid circles indicate calculations for the reference model at the right with a Moho depth of 32.5 km. Open squares indicate propagation from north to south and open triangles propagation from south to north.

Figure 15: Record sections of synthetic seismograms illustrating the effect of topography at the crust-mantle boundary. R reference structure; NS propagation from north to south; SN propagation from south to north. No scaling is applied with range.

INTRODUCTION

A number of the techniques which have been proposed for discriminating between different types of seismic sources at regional distances depend on the relative amplitudes of different P and S phases. Although the phase denoted in discrimination work as Lg is frequently the largest phase on a regional seismogram, it is known to be sensitive to variations in crustal structure. As a result attention has been transferred to Sn as a representative of the S wave radiation from the source, and comparison has been made with the Pn phase to characterise the P radiation.

However, detailed observations of the amplitude behaviour of Pn and Sn frequently show a very different dependence in the range 200 - 300 km away from the source. Whilst Pn is clear and separates distinctly from the rest of the P wavefield, Sn is often not discernable until distances around 300 km. Such behaviour has been observed on refraction surveys in Europe and from regional events in southeastern Australia.

In order to look at the causes of this behaviour and the way in which the Pn and Sn amplitudes vary with distance we have examined a wide range of long-range refraction profiles from the Eurasian area. We have also investigated the influence of topography at the crust-mantle boundary on the amplitude distribution to be expected from mantle phases such as Pn, Sn.

THE PHYSICAL CHARACTER OF REGIONAL PHASES

The analysis techniques used in discrimination work tend to label prominent arrivals on regional seismograms with simple descriptors (e.g. Pn, Pg, Sn, Lg) based in large part of the properties observed at regional arrays. However, in order to understand the way in which the relative amplitudes of such arrivals change with range we need to work with a more direct physical description of the propagation processes which give rise to the classes of regional arrivals.

Kennett (1989b) has shown how a description of the propagation processes involved in the major regional phases can be made in terms of reflection and transmission operators for propagation in a laterally heterogeneous medium. Figure 1 sketches the classes of ingredients which have to be taken into consideration in the representation of the mantle phases - both the propagation characteristics of the crust and the mantle have to be known for effective modelling. In addition the development of suitable computational approximations for such operators is dependent on a knowledge of the fine structure of the seismic arrivals.

The phase and group velocity definitions used for phases such as Pg, Lg do not fit in easily with the phase assignment schemes used by many location schemes, which are based on direct ray modelling of the possible propagation paths. However, with only a modest amount of effort, it has proved possible to modify the output of the new *iasp91* travel time routines which implement the travel time tables of Kennett & Engdahl (1991), to provide specific values of the phase and group velocities associated with the conventional phase names. An example of a script file generated by this process is displayed in figure 2. As has been previously noted by a number of authors (see e.g. Kennett 1985) the definition of Lg as a phase with a group velocity of 3.5 km/s is appropriate because of the

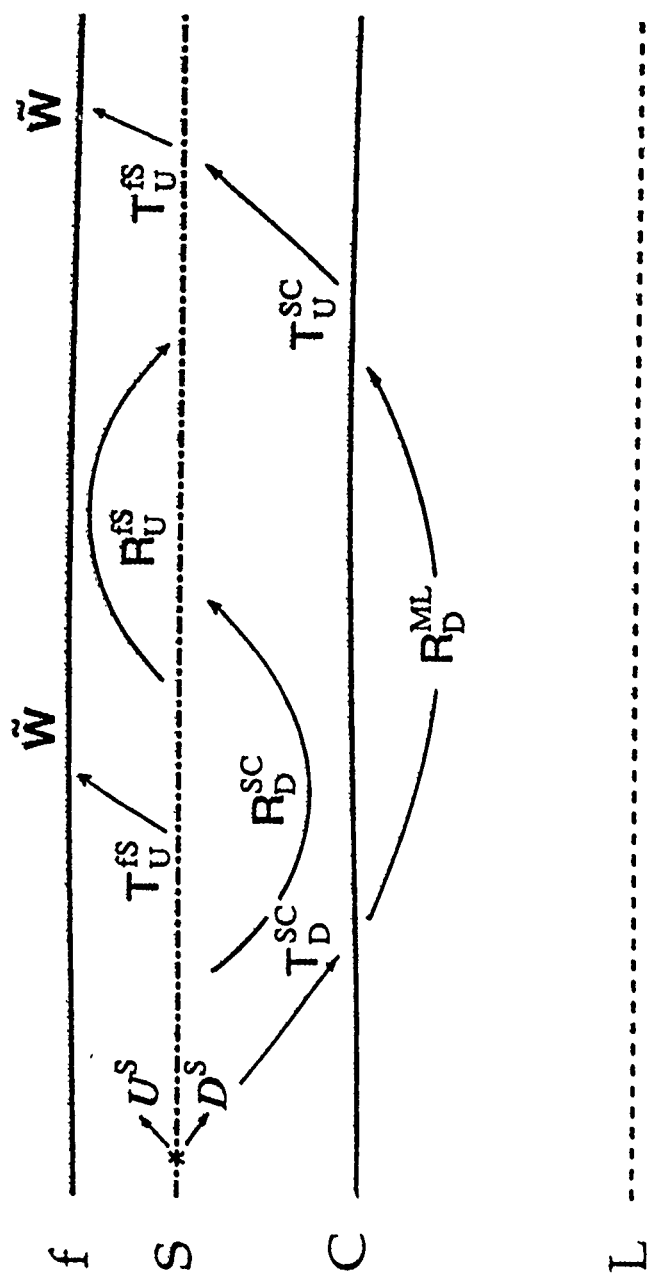


Figure 1: A schematic representation of the propagation processes which need to be included in the description of mantle phases (after Kennett 1989b).


```

Script started on Wed Aug 28 10:57:12 1991
% ttimr
enter model name:
iasp91
This routine for calculating travel times for
specific distances uses a set of precalculated
tau-p tables for theiasp91          model stored as
iasp91          .hed iasp91          .tbl

```

The source depth has to be specified
Phase list is preset for regional phases

You will have to enter a distance,
if this is negative a new depth is calculated
TO EXIT: give negative depth

Brnset: the following phases have been selected -

```

1 P
2 PKP      P
3 PKiKP
4 pPKP     pP
5 sPKP     sP
14 P'P'     PP
15 S
16 SKS      S
17 pSKS     pS
18 sSKS     sS
24 S'S'     SS
25 SP
26 PS

```

Source depth (km): 2

Enter range (km): 220

range	#	code	time(s)	slowness	group slow	ph vel	group vel
220.00	1	Pn	34.49	0.12369	0.15678	8.08	6.38
	2	pPn	34.97	0.12369	0.15896	8.08	6.29
	3	sPn	35.27	0.12369	0.16033	8.08	6.24
	4	Pb	36.71	0.15335	0.16688	6.52	5.99
	5	pPb	37.03	0.15335	0.16831	6.52	5.94
	6	sPb	37.38	0.15335	0.16992	6.52	5.89
	7	Pg	37.92	0.17235	0.17239	5.80	5.80
	8	sPg	38.41	0.17239	0.17461	5.80	5.73
	9	PbPb	39.85	0.15336	0.18112	6.52	5.52
	10	PnPn	42.01	0.12369	0.19095	8.08	5.24
	11	Sn	60.81	0.22246	0.27640	4.50	3.62
	12	sSn	61.60	0.22246	0.27999	4.50	3.57
	13	Sb	63.53	0.26581	0.28879	3.76	3.46
	14	sSb	64.07	0.26581	0.29122	3.76	3.43
	15	Sg	65.47	0.29752	0.29757	3.36	3.36
	16	SbSb	68.85	0.26583	0.31298	3.76	3.20
	17	SnSn	73.07	0.22248	0.33212	4.49	3.01
	18	PKiKP	994.30	0.00040	4.51953	2511.36	0.22
	19	P'P'df	2423.83	-0.00053	11.01740	-1882.37	0.09
	20	S'S'df	3272.17	-0.00041	14.87351	-2416.45	0.07

script done on Wed Aug 28 10:58:06 1991

Figure 2: Script file display for the adaptation of the iasp91 travel time routines to display phase and group velocities in order to compare the ray based assignments of conventional location procedures with the discrimination phases Pg, Ig.

mutual interference of many multiple S reflections within the crust, but this means that a phase association via ray definition will shift quite rapidly between different phases with distance. A similar problem tends to happen with S_n as the distance increases, the amplitude of the waves returned from the mantle diminish and fall below the coda of P, but the surface multiples remain visible and can be confused with the true arrival S_n (Kennett 1985). The reinforcement of the surface multiples occurs because there are a number of different physical propagation paths which have the same time behaviour.

In addition, the generic descriptions P_n , S_n used for mantle phases are not necessarily an accurate description of the character of the arrivals which are actually picked from a regional seismogram. As we shall see below, long-range refraction experiments ascribe significant substructure to the " P_n " arrival between 200 and 800 km. The interaction of these multiple arrivals from the mantle and surface multiples gives a complex structure of propagation processes which are reflected in the visual complexity of regional seismograms.

An inexpensive and convenient tool for assessing the way in which different types of propagation effects can interact to build up the patterns seen on an individual seismogram is provided by WKBJ seismograms (Chapman 1978) for a horizontally stratified model. Unlike methods based on the full reflection response of the medium, the different classes of propagation paths have to be specified separately. As a result there is a significant initial effort in assembling the ray code descriptions which control the class of physical processes which are included, but once this is done the computation of seismograms is very rapid. Further there is no difficulty in isolating the contribution of different processes by modifying the choice of ray codes. An example of the WKBJ synthetics for a simple crustal model representative of a shield region is presented in figure 3, together with the group velocity trajectories associated with the array definitions of P_g , L_g . As expected these trajectories cut across a sequence of multiple arrivals representing P and S wave reflections within the crustal waveguide.

For this WKBJ example the ray codes were chosen so that up to 4 surface multiples of each major ray path would be included. This includes reflection from each of the boundaries in the model or refracted (diving) waves below interfaces. The theoretical seismograms are presented with trace normalisation, and clearly display the significance of multiples of the mantle phases at greater distance. The multiple reflected waves in the crust tend to asymptote to the expected trajectory of L_g and we can see that we would expect systematic errors from the group velocity definition of L_g for distance ranges close to the critical point of successive multiples of the reflection from the crust mantle boundary. As more and more multiples contribute to the wavefield the association of the maximum S amplitude with the specific group velocity of L_g improves. However for epicentral distances less than 400 km it would be preferable to attempt to associate the observed L_g arrival with the theoretical times for S_g or $S_g S_g$.

It may be possible to introduce a partial allowance for lateral heterogeneity into the WKBJ calculation by introducing systematic perturbations to the central phase functions which are currently constructed for horizontally stratified model. Such a procedure will be investigated over the next year.

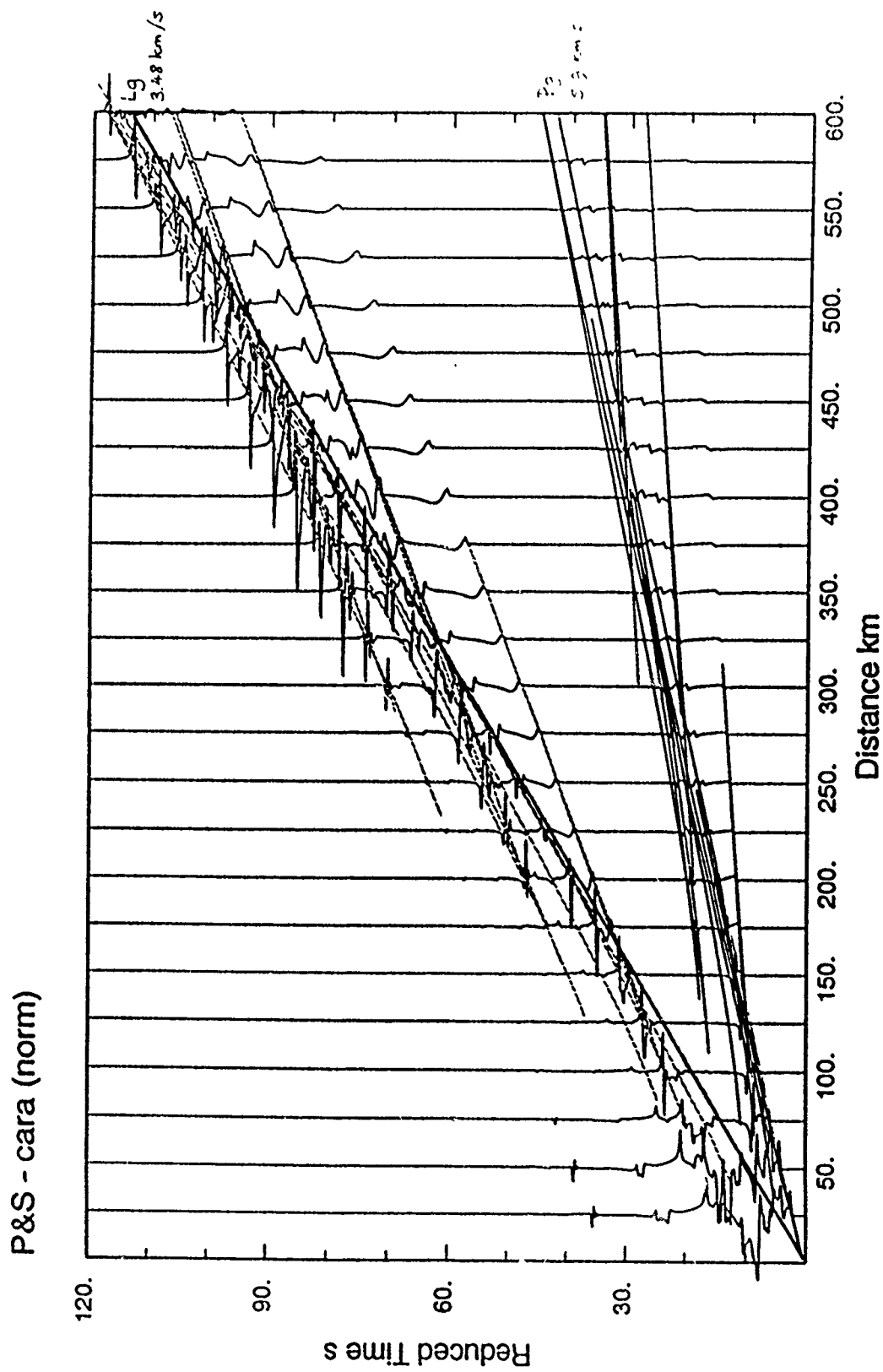


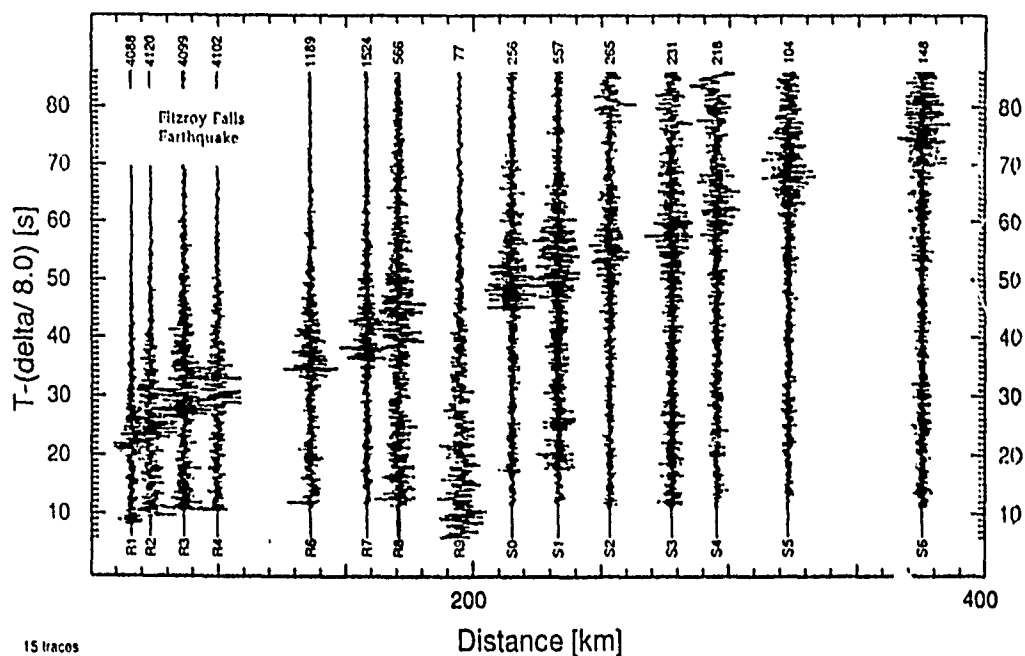
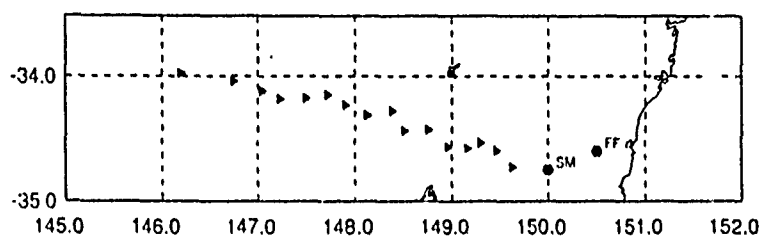
Figure 3: WKBJ synthetic seismogram for a simple crustal model representative of a shield region. Up to 4 crustal multiples are allowed for reflection from each interface or for diving waves. The P and S wave calculations were carried out separately and superimposed in plotting.

OBSERVATIONS OF MANTLE PHASES

A number of authors have noticed that the onset of the Sn phase around 200 km can be difficult to pick by comparison with the equivalent Pn phase even for those situations where the P coda is low. These observations come from a wide range of stable tectonic environments. For example, the phase association procedure used for locating earthquakes in southeastern Australia only declares an Sn phase when the estimated distance is greater than 300 km because of the difficulty in obtaining reliable picks at shorter distances. The amplitude of the energy return from the mantle is dictated by the size of the velocity gradients for P and S waves in the uppermost part of the mantle. The pattern of observations for Sn with a low amplitude arrival around 200 km but greater amplitude at ranges beyond 300 km, suggests that the S wave gradient is low in the uppermost mantle and then increases at a depth of 10 or so kilometres below the crust-mantle boundary. Recently Gajewski et al (1990) have shown that this pattern of slow emergence of Sn is observed on many refraction profiles in western Europe in zones with a similar geologic setting to Eastern Australia i.e. regions affected by mountain-building episodes in the last 300 Ma. They have associated the differences in velocity gradient for P and S with a possible differences in mineral composition with depth. Such geologic environments also occur in much of the Soviet Union. As we shall see later in some areas of precambrian rocks Pn and Sn are observed with comparable clarity, so that there may well be differences in the nature of the uppermost mantle which depend on the geological history of the region being studied. Gajewski et al (1990) also noted differences in the character of Sg phases compared with the corresponding Pg arrivals.

There are only a limited number of experiments in which both P and S propagation can be tracked to significant distances with a station spacing close enough for the evolution of the wavefield to be judged. Most of these cases are for explosions, but there a very limited number of earthquake observations. During the operation of a linear array of seismographs in southeastern Australia during the southern summer of 1989/1990 we were fortunate to record both an earthquake (FF) and a quarry blast (SM) which lie along the line of the profile. The corresponding record sections are displayed in figure 4 together with an inset map of the array configuration. The general character of the wavefield is very similar although there are differences in the P radiation (by accident a nodal plane for P wave radiation from the Fitzroy Falls earthquake passes through the line of the array). On each section we can see the change in phase velocity with the emergence of the Pn arrivals but the corresponding emergence of the Sn phase cannot be reliably tracked. The amplitude of the P coda is quite high and there is little difference in frequency content between the P and S wave fields. This example gives a good illustration of the merits of multi-station recording. Where close station spacing was achieved there is a good correlation of the records at successive and phases can be readily identified. Even for the isolated distant station identification of arrivals is simplified by extraction from closer distances. In the first period after the installation of a new regional station it would be highly desirable to build up a record section from available sources so that the structure in the neighbourhood of that station can be calibrated.

RAG 89/90



15 traces

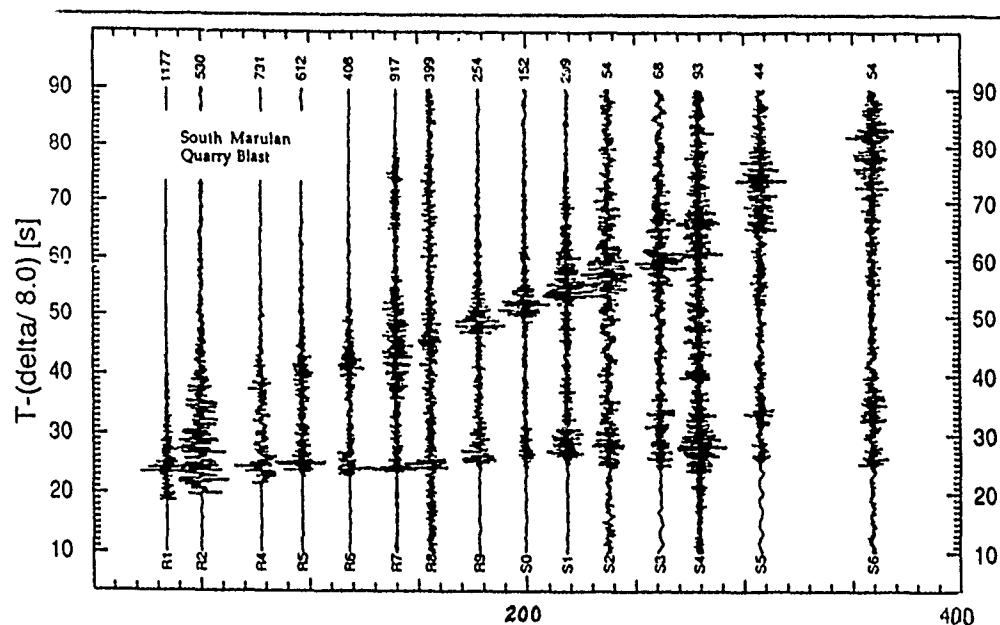


Figure 4: Recordings of an earthquake (FF) and a quarry blast (SM) along the same array of portable seismographs in southeastern Australia. In each case the Pn phase can be clearly observed even though the earthquake phase are close to a node for P, it is much more difficult to detect the Sn arrival even with a number of records.

A further example of a detailed set of earthquake observations at regional ranges is provided by the recording of an earthquake in Scotland during the long-range refraction experiment conducted in 1974. The earthquake was displaced from the line of the profile but there is still a very useful set of observations from 70 to 290 km away from the event (figure 5). There is a clear mantle S arrival with a rather emergent onset which in this case can be tracked back to the cross over with the Sg phase. Figure 5 displays the onset of both the P and S wave portions of the wavefield as recorded on vertical component seismometers. The travel times superimposed on the S wave section are derived from a model of the crustal P wave velocity determined by refraction work by assuming a ratio of P and S velocities of $\sqrt{3}$. These theoretical times are in reasonable agreement with the S wave section, though the predicted times for Sn may be a little early. The general character of the P and S fields is similar but in this case the ratio of the mantle to crustal amplitudes is larger for S than P.

In order to see whether the pattern of propagation of the mantle phases is consistent from region to region and also to investigate the evolution of the Sn/Pn amplitude ratio with distance we have searched for refraction recordings with good S wave arrivals in the distance range from 100 - 1000 km. Although much of the long-range profiles in Europe were originally recorded with three-component sensors, most of the interpretations have been based on the P wave data from the vertical component records and relatively few S wave sections have been published. However, sufficient S wave data exists for us to be able to begin to make a comparison of the propagation characteristics of the P and S wave field.

As an example we present in figure 6 a comparison of P and S recordings at ranges from 200 - 800 km (Hirn, 1977) from a profile of instruments deployed across France to record a large explosion fired in the sea off Brest. The record sections are phased to concentrate attention on the mantle arrivals which in nuclear monitoring work we would normally term Pn and Sn. However we can see clearly from figure 6 that such phases have significant substructure and the almost constant apparent velocity is built up from a sequence of en-echelon phases which progressively become first arrivals as the distance increases. The interpretation of such arrivals in terms of a one-dimensional velocity model leads to very complex velocity distributions with multiple low-velocity zones (see e.g. Kind 1974), but it is very likely that much of the complexity arises from lateral heterogeneity in the structure in the upper most mantle (Fuchs & Schulz, 1976). A similar pattern of complex structure within the wavegroup characterised by Pn can be seen in the record sections presented by Yegorkin & Chernyshov (1983) from peaceful nuclear explosions in the Soviet Union (fig 13).

In figure 7 we illustrate the pattern of rays associated with the class of model which has been proposed to explain the complexity of the observed mantle arrivals. A weak gradient zone below the Moho is terminated by a low velocity zone (which is needed to get a suitable delay for arrivals from greater depth). This leads to a relatively weak Pn arrival from the uppermost mantle which is supplanted at greater distance by the P_I phase returned from depth, and at even greater ranges by P_{II}. The observations of Gajewski et al (1990) relate to the Pn, Sn arrivals from the uppermost mantle and not to these arrivals from greater depth. The arrivals P_I, P_{II}, S_I, S_{II} are frequently more energetic and are the phases which

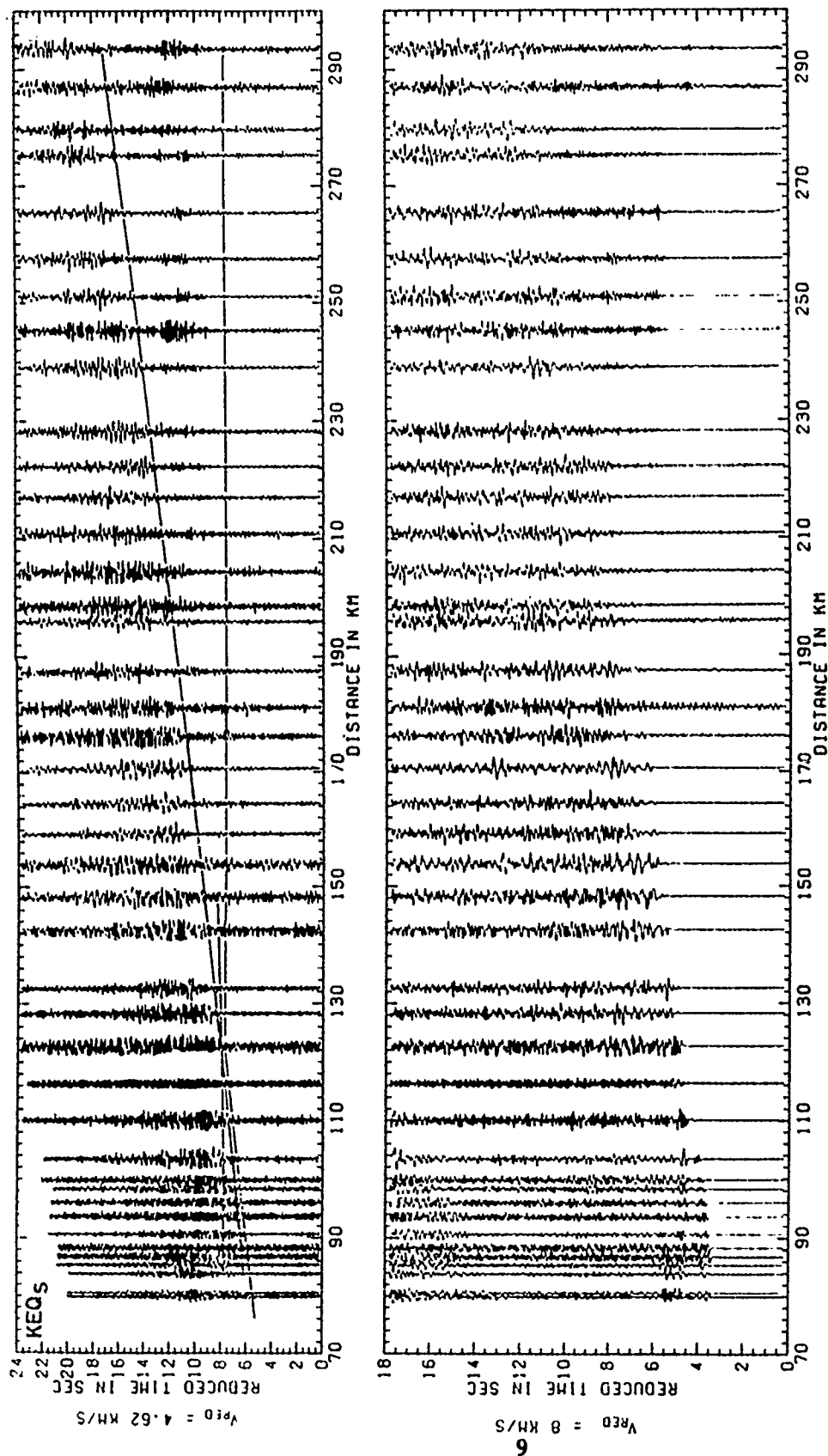


Figure 5: P and S wave sections for the vertical component of displacement for an earthquake in northwestern Scotland recorded during the long-range refraction profile through the British Isles. The reduction velocity for the P section is 8 km/s, and for the S section it is 4.62 km/s (after Kaminiski et al 1974).

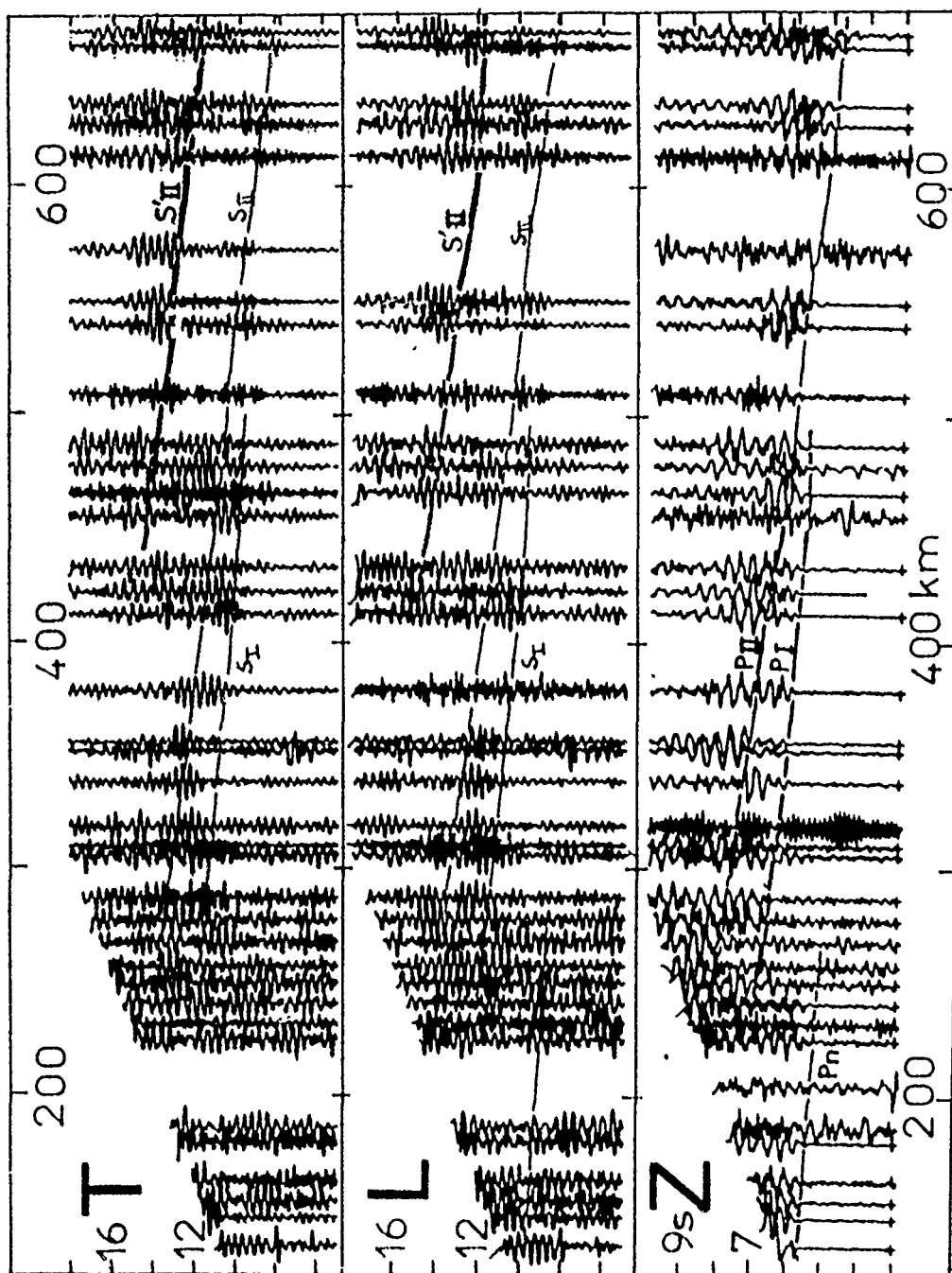


Figure 6: Three component record sections for a large explosive shot off the French coast recorded across a long range profile in France (after Hirn 1977). Reduction velocity for the Z section is 8 km/s, whereas for the L and T sections the velocity is 4.62 km/s

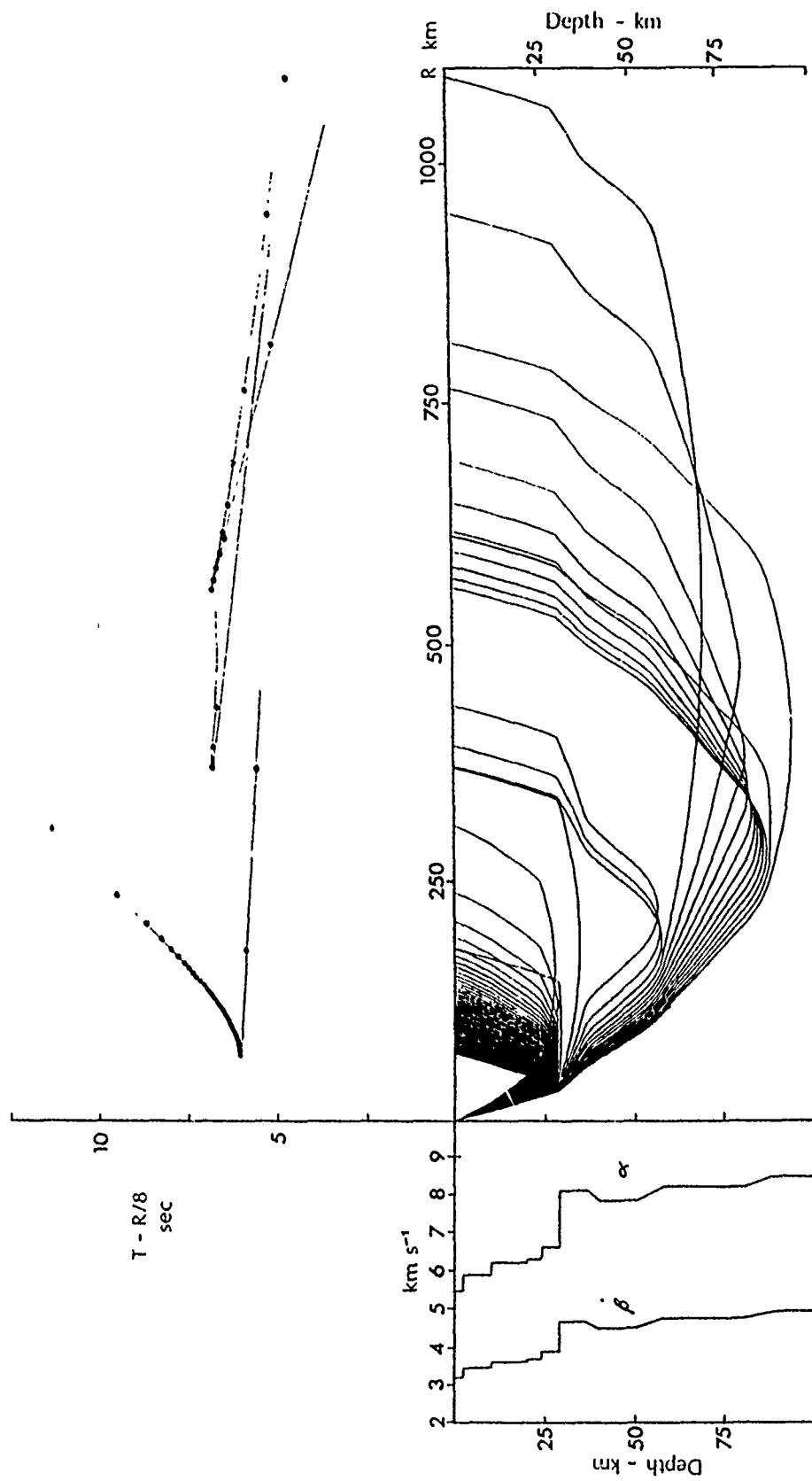


Figure 7: Ray diagram illustrating the way in which a mantle structure with a number of gradient zones can give rise to a sequence of phases returned from the mantle with an apparent en-echelon behaviour in time.

would be designated in discrimination work as Pn, Sn because an individual seismogram is not sufficient to recognise the substructure of the wavefield.

In general the quality of S data from explosive sources is not very good because the P coda is energetic and so we are looking for S arrivals against a relatively noisy background. However some experiments, especially in Precambrian terrains where the shear velocities are relatively high, do give a very good representation of the S wavefield even on vertical component instruments. Figure 8 shows the locations of three refraction profiles in Fennoscandia which have good quality S arrivals.

Figure 9 shows P and S wave sections from the same shotpoint point A in a Finnish-Polish refraction experiment SVEKA across part of the Baltic Shield in southern Finland (Luosto et al 1984, Grad & Luosto 1987). The S arrivals are very clear and give a good general agreement with the pattern of the P arrivals. In this case the crust is rather thick and the transition from Moho reflections to refractions occurs at the end of the profile. Interestingly the reflection from the Moho around 160 km offset is clearer on the S wave section. Rg is only visible to 100 km.

The quality of the S records in figure 9 is surpassed by the remarkable set of records from a further Finnish-Russian experiment BALTIC which lay further to the southeast (closer to the Russian border). The data from shot point B is shown in figure 10 and at first sight is difficult to distinguish which is the P and which is the S profile (other than by examining the timing of the Rg phase). The correspondence of the phases is exceptionally close and here, at least, there is a very distinct Sn arrival beyond 200 km. The reversed profile from shotpoint G has less clear Pn and Sn arrivals with a cross over around 3020 km. Despite the pronounced topography on the Moho (see e.g. Bannister, Ruud & Husebye 1991), good mantle arrivals are seen on these profiles.

A further experiment in northern Finland and Sweden, the POLAR profile (Luosto et al 1989) shows uniformly good S propagation from all shot points including those with fairly small charges. A record section from shotpoint A at the southern end of the line is shown in figure 11. In this area it would appear that the Moho is very sharp because of the very distinct PmP, SmS arrivals which can be seen to connect directly into the Pn, Sn phases at greater distance. This profile lies relatively close to the Arcess array for which there are generally very clear observations of S phases from the mine blasts on the Kola peninsula. This geologic province is the oldest in Fennoscandia and it would appear that attenuation is rather low.

A comparison of the three sets of P and S record sections presented in figs 9-11 shows noticeable differences in the character of the wavefield. For the SVEKA profile (fig 9) there are strong direct Pg and Sg phases extending out to 200 km, where they are overtaken by the Pn and Sn phases. The reflection from the crust mantle boundary is more distinct for S than for P, indeed it is quite difficult to correlate the P wave arrival to distances smaller than 180 km where the corresponding S reflection is very clear.

For the BALTIC profile (fig 10) which is again in southern Finland, Pg and Sg are clear but by comparison less energetic than for SVEKA. In this case both the prograde and retrograde travel time branches associated with reflection and refraction at the crust-mantle boundary can be clearly seen for both P and S. The

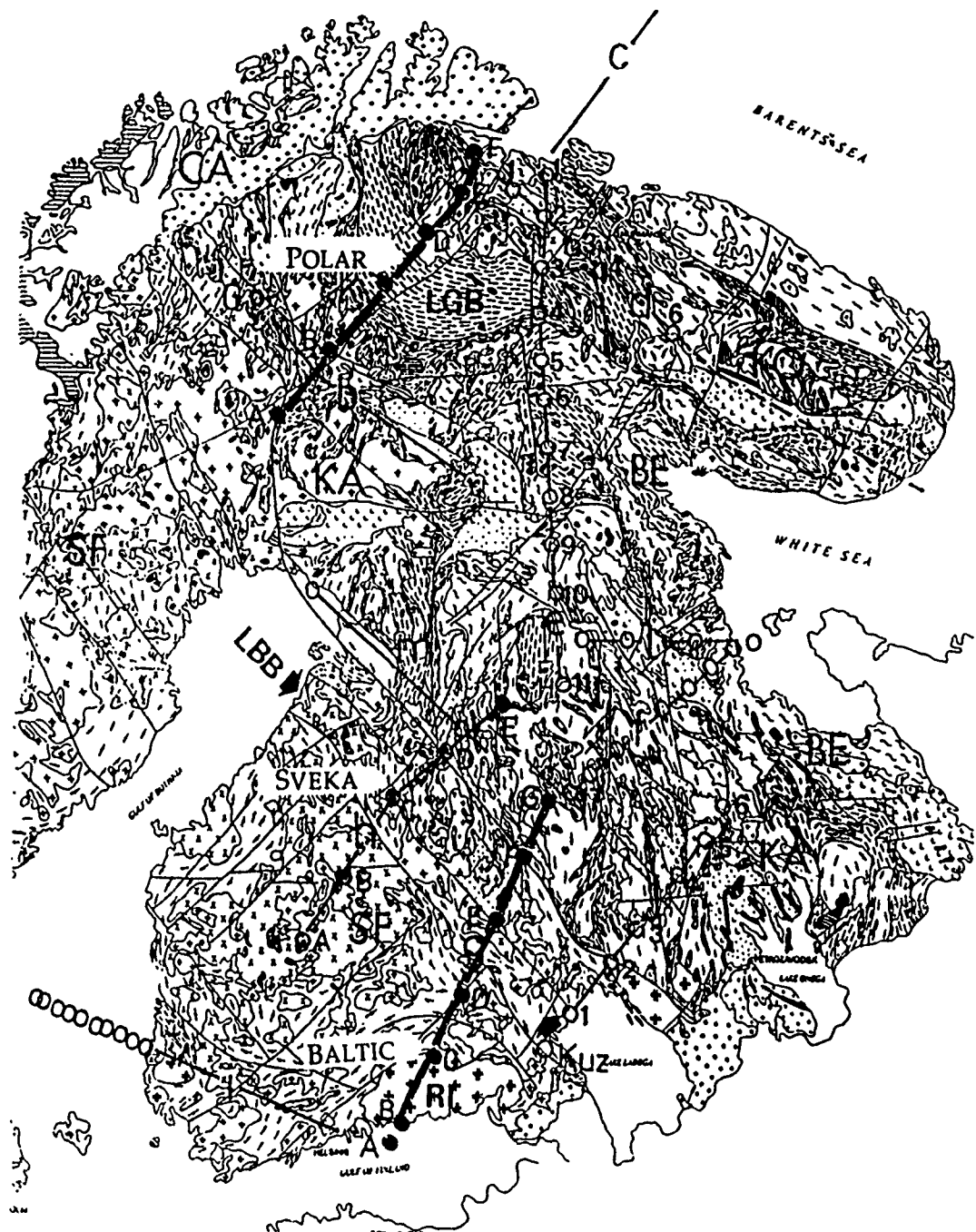


Fig. 1. DSS profiles: *b* = Finlap; *c* = Barents Sea; *d* = Pechenga-Umbozero; *e* = Pechenga-Kostamuksha; *f* = Kem-Tulos; *g* = Baltic; *h* = Sveka; *i* = Sylen-Porvoo; *j* = Ladoga; *k* = Polar; *l* = Kem-Uchta; *m* = Eljäärvi-Lahnaslampi. *SF* = Svecofennian Domain; *KA* = Karelian; *BE* = Belomordian Province; *KO* = Kola Peninsula Province; *CA* = Caledonides; *LGB* = Lapland Granulite Belt; *LBB* = Ladoga-Bothnian Bay Zone; *RI* = Viborg Rapakivi Granite Intrusion (tectonogeological map by Korsakova et al., 1987).

Figure 8: Configuration of the SVEKA and BALTIC and POLAR refraction experiments in Fennoscandia.

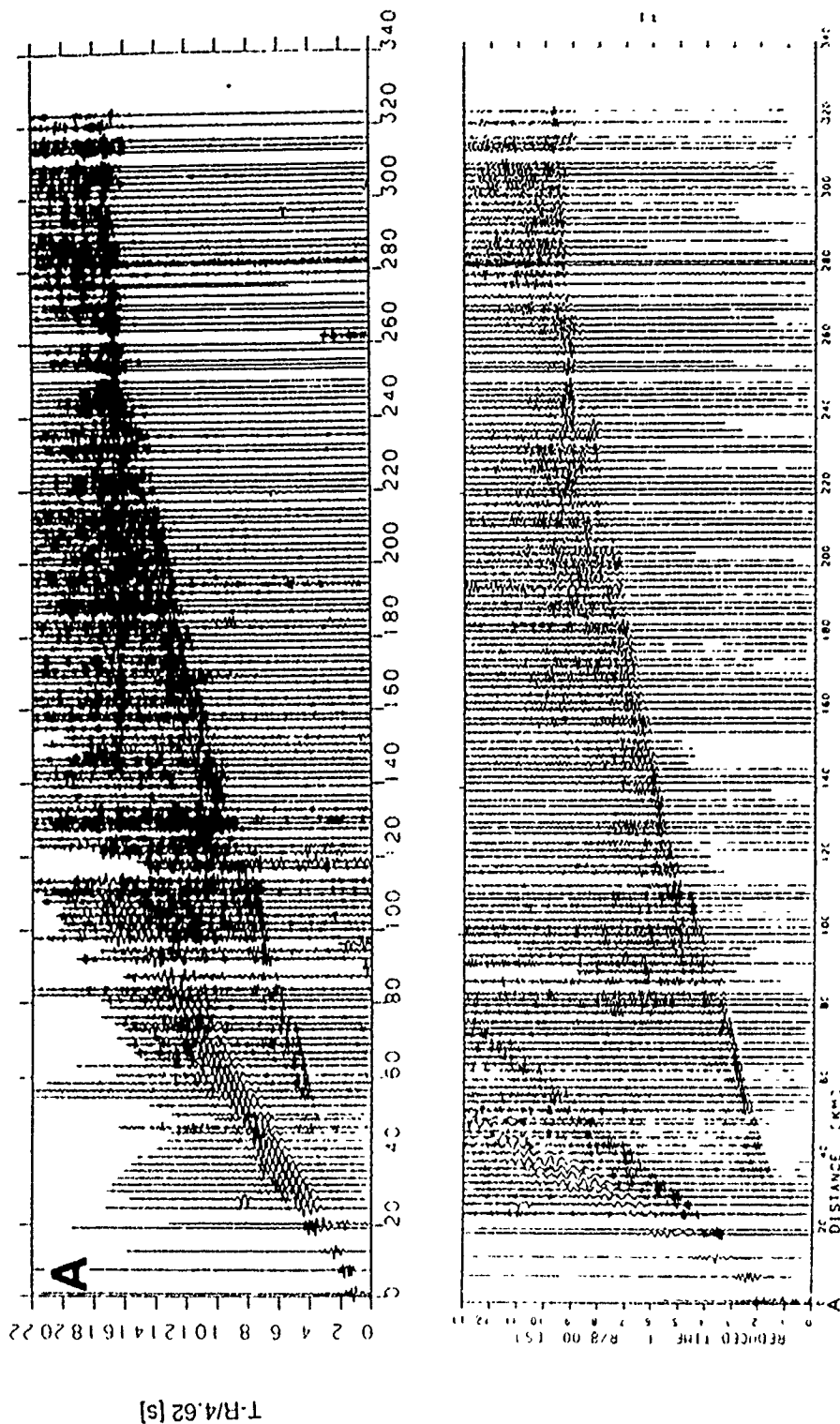


Figure 9: Comparison of P and S record sections from the SVEKA refraction profile in Finland using vertical component seismometers, the traces are amplitude normalised. The reduction velocity for the P section is 8 km/s, and for the S section it is 4.62 km/s (after Luosto et al 1984, Grad & Luosto 1987).

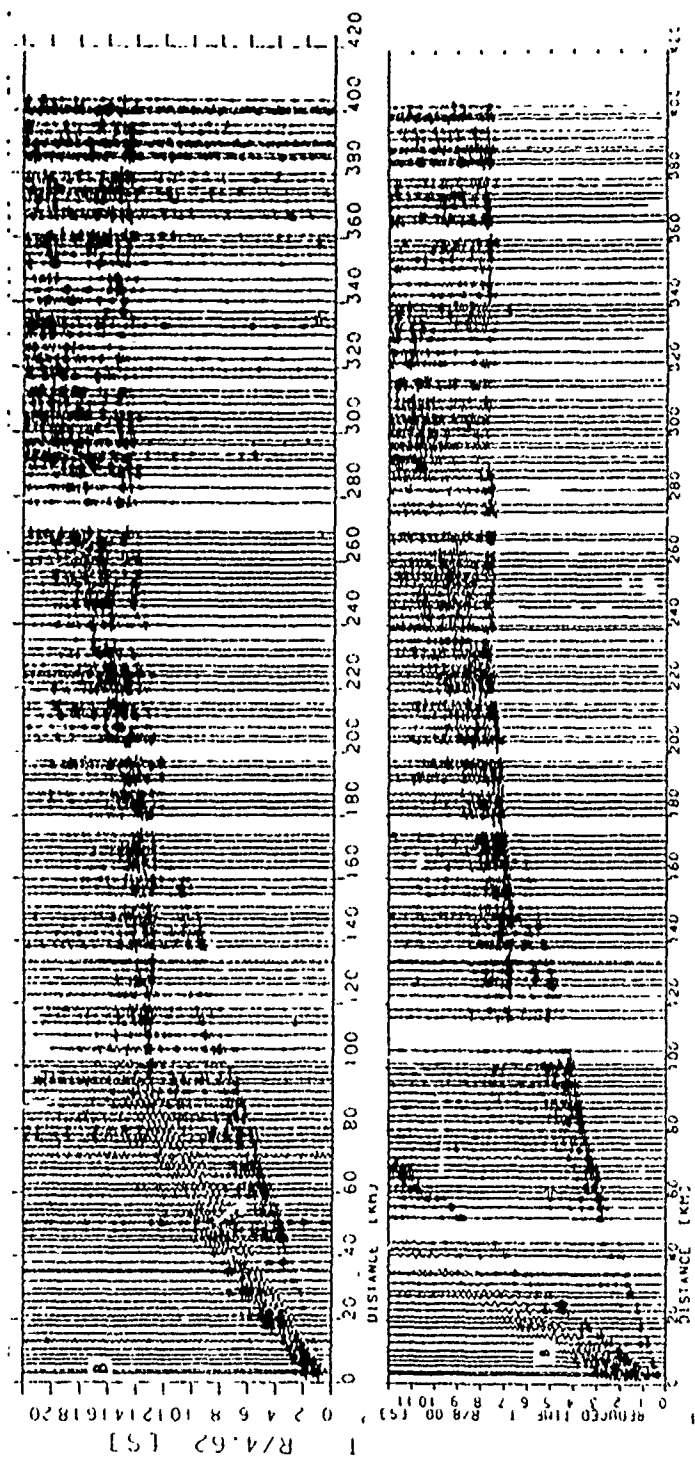


Figure 10: Comparison of P and S record sections from the BALTIC refraction profile in Finland using vertical component seismometers, the traces are amplitude normalised. The reduction velocity for the P section is 8 km/s, and for the S section it is 4.62 km/s

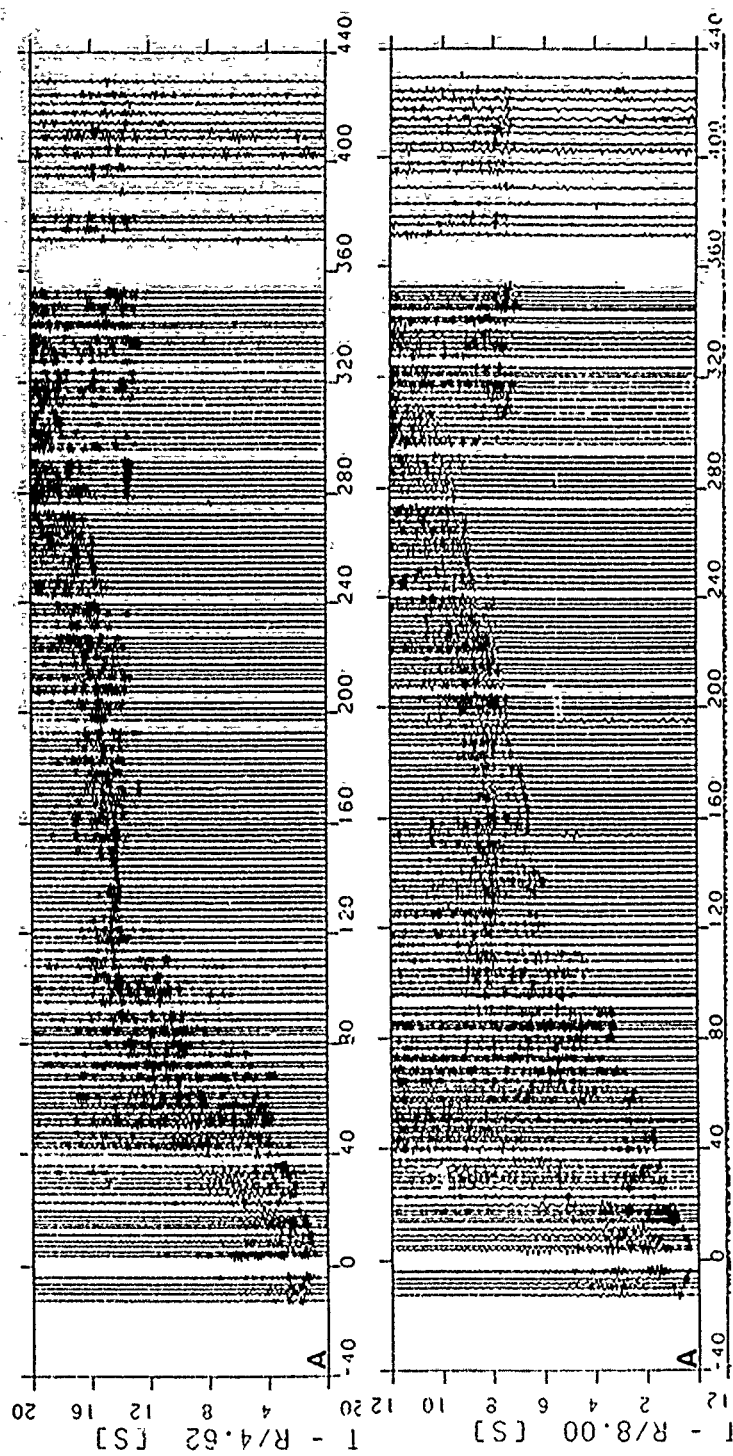


Figure 11: Comparison of P and S record sections from the POLAR refraction profile in northern Fennoscandia using vertical component seismometers, the traces are amplitude normalised. The reduction velocity for the P section is 8 km/s, and for the S section 4.62 km/s (after Luosto et al 1989).

strength of the mantle arrivals near the crossover at 180 km leads to strong suppression of the Pg and Sg arrivals in these amplitude normalised displays.

For the POLAR profile (fig 11) the exceptional strength of the reflected energy from the Moho suppresses the display of Sg, in particular between 120 and 160 km. If a phase association were to be made in this case on the maximum S amplitude it would be displaced by 2-3 seconds from the assumed trajectory for lg and could well lead to significant mislocation of an event. The mantle arrivals are weaker than for the BALTIC profile and we can see the Pg and Sg arrivals grade into the PmP and SmS arrivals as would be predicted by standard crustal models.

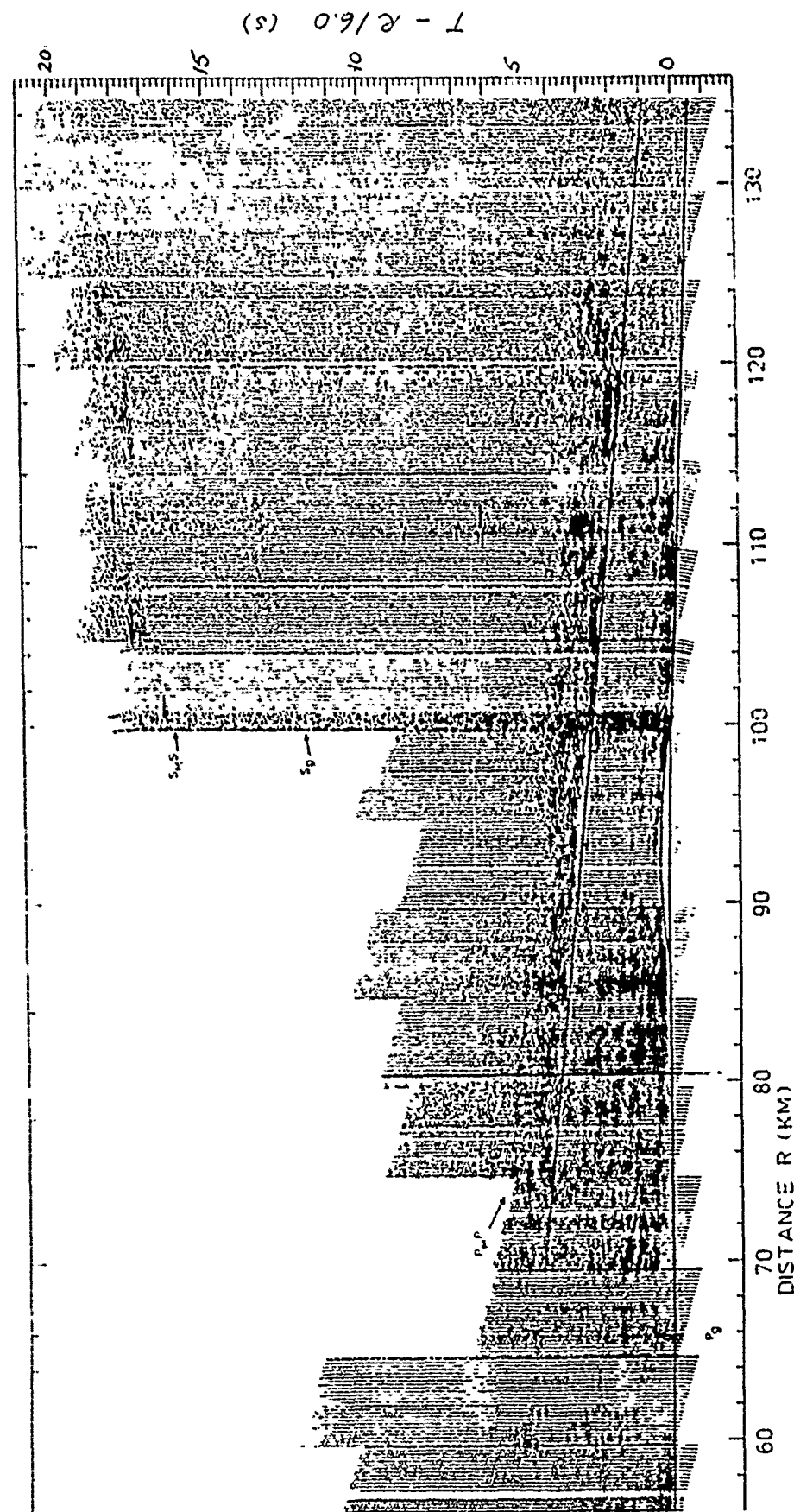
The map of refraction profiles in Fennoscandia indicates a number of profiles within the Soviet Union, with a relatively dense shotpoint spacing. Unfortunately almost all the Deep Seismic Sounding experiments carried out within the USSR have used analogue recordings. Relative close station spacing e.g. 100 m with a 5 km recording spread has enabled close correlation of features on the seismograms. Attention has largely been focussed on the time relations of the different features and in published accounts only very limited descriptions of the amplitude behaviour are provided. It is therefore quite difficult to extract systematic information on the character of the wavefield.

A very interesting experiment was carried out by Jentsch (1979). He hand digitised a very large number of Russian recordings from a DSS profile in the southern Ukrainian shield, and then attempted to apply conventional one-dimensional interpretation techniques to this data. Figure 12 displays a portion of the record section which displays both the P and S energy. The source for the recordings were multiple explosive charges in separate holes. A notable feature of these records is the relatively short correlation distance for the amplitude along individual phases. Although general trends are clear, there are significant variations in amplitudes over distances little larger than the aperture of a regional array of the Noress/Arcess type; these often correlate between the P and S phases but do not always coincide in range. We therefore certainly need to be cautious in interpreting amplitude ratios between different phases from individual seismograms. For discrimination purposes the stability of an amplitude ratio estimate based on a number of closely spaced stations is certainly to be preferred to even a single three component station. Mini-arrays with a few vertical component sensors surrounding a central three-component systems would seem highly desirable in this context.

Yegorkin & Chernyshov (1983) have presented record sections for P waves along DSS profiles in northern Siberia (to 1700 km) and central Asia (to 900 km). The typical spacing of traces is to 10 km and a portion of the Siberian line is reproduced in fig 13. The patterns of P wave propagation for the onset of the seismogram are similar to those seen on long-range refraction profiles in Europe. The energy return from the mantle consist of a number of distinct arrivals which can be correlated over substantial distances. It would appear that the recording interval used in these very long range refraction experiments was too short to include the S arrivals from the mantle as well.

THEORETICAL STUDIES

In association with the observational studies we have also considered ways in which the behaviour of the Pn and Sn can be modelled with allowances for the



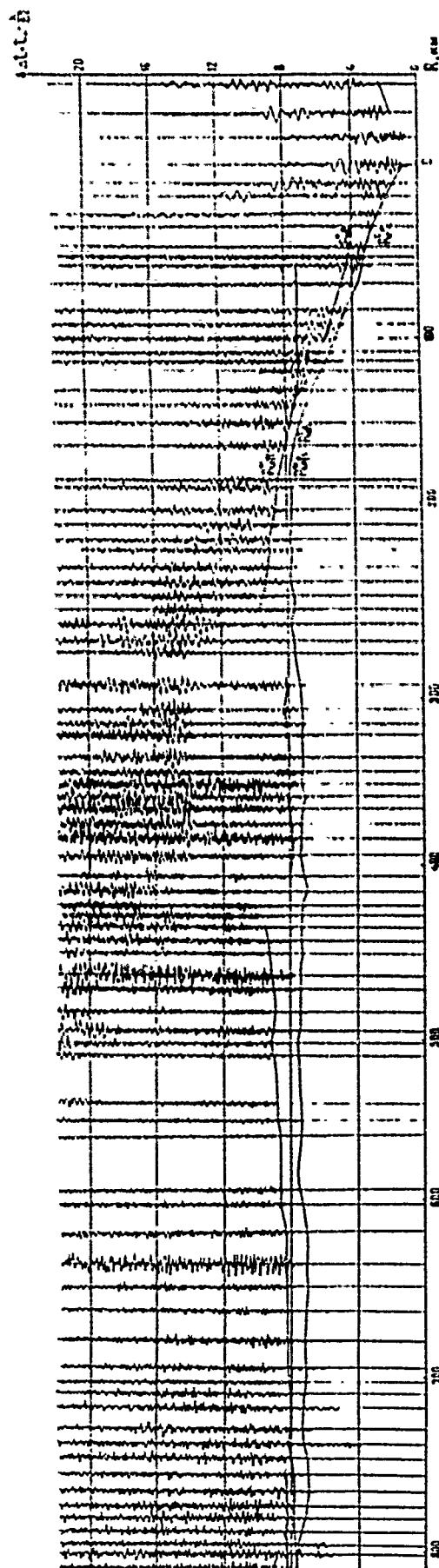


Figure 13: Portion of the record section from a DSS profile in northern Siberia, the reduction velocity is 8.2 km/s (after Yegorkin & Chernyshov 1983).

effect of lateral heterogeneity. As we have seen above, we cannot neglect the influence of free surface multiples and so we cannot easily separate the modelling of mantle phases from the problem of wave propagation in the crustal waveguide.

For S_n we can adapt the coupled mode scheme previously used by Kennett (1986) for modelling L_g wave propagation in the crust with allowance for coupling to S_n , by simply enlarging the number of modes considered and thus the phase velocity span which can be modelled. For propagation up to 3-4 Hz this would require coupling calculations spanning up to 200 modes (i.e. 200 coupled complex differential equations). Such calculations are feasible for many frequencies on a supercomputer but are rather time consuming, and even so we are restricted to slight perturbations of the crust-mantle boundary.

In principle, the mode coupling procedure can also be extended to the P_n and P_g parts of the wavefield but this would require more than a 1000 modes for frequencies higher than 2 Hz and as such does not present an attractive route. If full account is taken of the possibility of reflection we would need to solve a differential equation for a 1000×1000 complex matrix: even with the most efficient algorithms this would be very difficult on current computers.

We have therefore been looking at alternative representations of the seismic wavefield which exploit the idea of coupling between different horizontal wavenumbers (which underlies the mode coupling procedure) but which use an alternative expansion of the field in orthogonal functions. A suitable basis set exists if the free surface can be neglected and so could be used for propagation to around 300 km. However no satisfactory solution has yet been found to allow inclusion of surface reflections. We will continue to investigate methods for modelling the propagation of the mantle phases over the next year.

One aspect of the character of P_n and S_n which has proved amenable to modelling is the influence of topography at the crust-mantle boundary. In the Finnish example above there is substantial topography at the Moho, and the long-range refraction profile along the length of the British Isles (Bamford et al, 1976) has also shown significant topography at this level. For high frequency waves, an approximation to the effects of an irregular boundary can be made by introducing a generalised transmission coefficient whereby a single incident plane wave couples into a spray of plane waves on the other side of the interface.

This approach can be introduced into a modification of the reflectivity method, in which ray techniques are used to transfer energy from the source to the irregular boundary and from that boundary to the receiver; but a full calculation is made in a horizontally layered structure lying beneath the crust-mantle boundary. However, the amplitude kernel in the plane wave response for this region is modulated by the redistribution associated with the generalised transmission coefficients on entry and exist from the mantle. The method assumes that the top of the reflection zone averages to a flat level assumed in the reference model; this can give rise to slight inaccuracies in the amplitude and timing of waves reflected at the underside of the interface. The dominant arrivals corresponding to diving waves will be correctly represented.

The amplitude distance behaviour for a model derived from the Moho topography of Bamford et al (1976) is displayed in fig 14, together with the form of the crust-mantle interface for propagation from north to south and from south to north. These amplitudes are compared with those calculated for a laterally

uniform reference model and have been derived from the synthetic seismogram sections in Figure 15, which have been calculated using a phase velocity window from 8.1 to 10.0 km/s in all cases. This window corresponds to purely propagating waves in the layer immediately below the crust-mantle interface and allows direct comparison between flat and perturbed topography at the Moho.

The results for the reference model (with horizontal layering and a Moho depth of 32.5 km), are indicated in fig 14 by the solid circles, open squares are used for propagation from north to south, and open triangles are used for propagation from south to north. The fluctuations introduced by the presence of topography are significant but in general less than the typical variability in observed amplitudes. The offset distance from the Moho to the recording point at the surface is about 45 km, so the amplitude symbol will be displaced from the relevant topography. The major change from the reference model is a shift of the amplitude peak near 300 km to shorter distances and an enhancement of the amplitude minimum near 400 km range.

These features are clearly seen in the record sections of the theoretical seismograms in fig 15. The effect of topography is to give a pronounced concentration of energy near 300 km accompanied by reduced amplitudes near 400 km. If we were to interpret the NS and SN record sections in terms of horizontally stratified models, we can see that the resulting velocity models would differ significantly from the reference models. In particular, to change the peak in P_1 amplitudes a more pronounced velocity inversion would be required.

These calculations show the effect of topography on the P wavefield, and we can anticipate similar effects for S waves. However, unless the velocity ratio between P and S waves is a constant throughout the medium, the propagation paths for P and S waves will differ. The focussing and defocussing effects associated with topography can therefore be displaced slightly between the P and S wave patterns which will give rise to fluctuations in the ratios of amplitudes of mantle P and S waves and so complicate use as a discriminant.

CONCLUSIONS

We have been able to demonstrate that the amplitude behaviour of P_n and S_n with distance is quite complex and that it is necessary to look at the anatomy of the phases in order to understand the potential performance of some regional discriminants. In detail the P_n and S_n phases tend to break up into a sequence of overlapping branches associated with fine structure in the upper part of the lithosphere. Anomalously low S_n amplitudes can arise between 200 and 300 km away from the source.

The current class of regional phase discriminants based on averaged behaviour of seismic phases such as P_n and S_n could give misleading results in some distance ranges because of the way in which the peak amplitudes in the requisite time windows shift between different wave groups. Such effects are difficult to pick up from isolated earthquakes or mine blasts but are evident in long range refraction profiles or comparable record sections.

It will be difficult to assess the amplitude behaviour of the P_n and S_n phase for the area around a particular receiver site without careful calibration, and the analysis of regional phases will need to be adapted to take the nature of the particular phases into consideration. The maximum amplitude within a

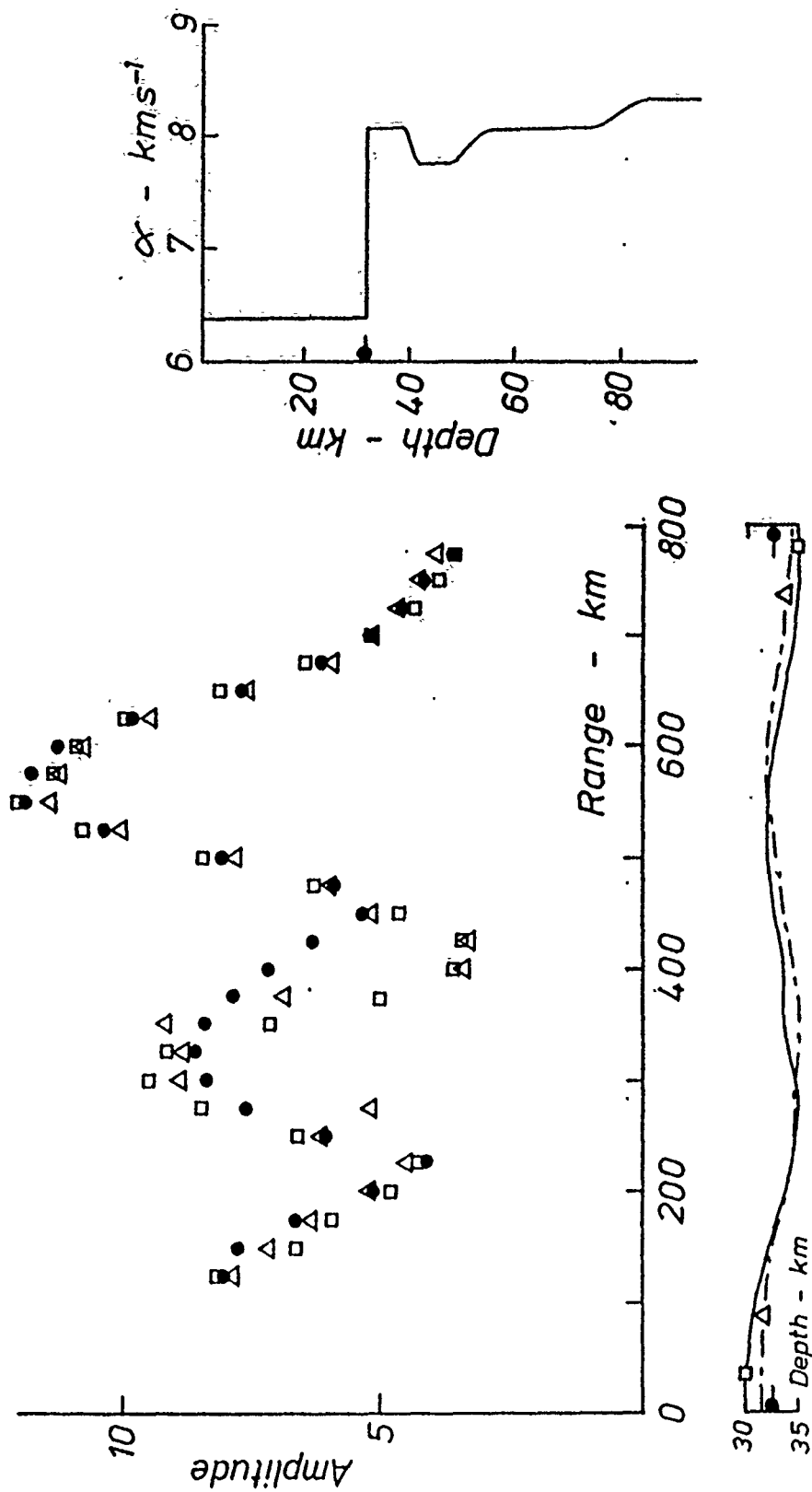


Figure 14: Amplitude distance behaviour for topography at the crust-mantle boundary. Solid circles indicate calculations for the reference model at the right with a Moho depth of 32.5 km. Open squares indicate propagation from north to south and open triangles propagation from south to north.

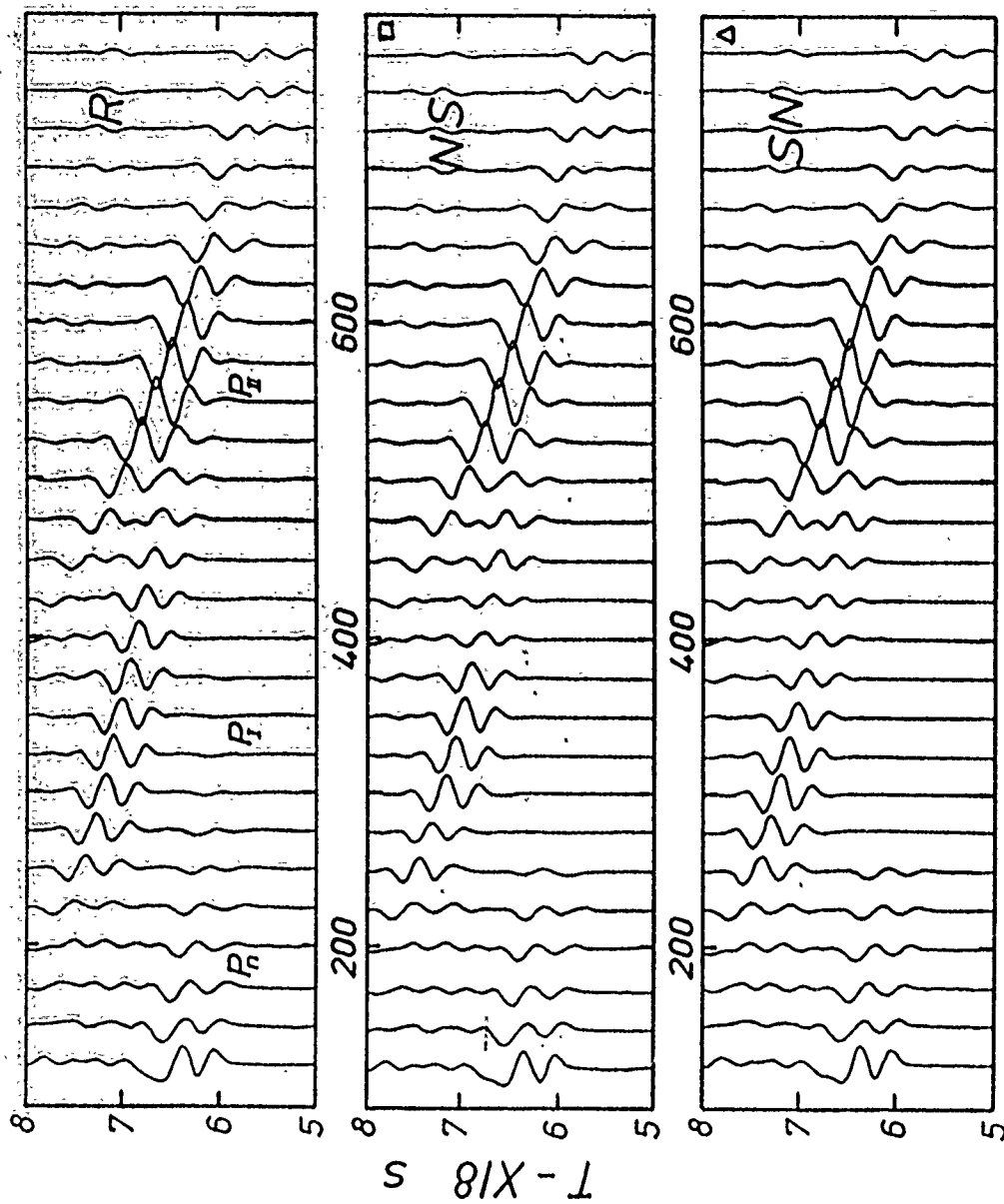


Figure 15: Record sections of synthetic seismograms illustrating the effect of topography at the crust-mantle boundary. R reference structure; NS propagation from north to south; SN propagation from south to north. No scaling is applied with range.

specified group velocity window may not be the best measure of the P or S wave content of the seismogram.

REFERENCES

- Bamford D., Faber S., Jacob B., Kaminski W., Nunn K., Prodehl Co., Fuchs K., King R. & Willmore Pl, 1976. A lithospheric seismic profile in Britain - I. Preliminary results, *Geophys. J. R. astr. Soc.*, **44**, 145-160.
- Bannister S.C., Ruud B.O. & Husebye E.S., 1991. Tomographic estimates of sub-Moho seismic velocity estimates in Fennoscandia and structural implications, *Tectonophys.*, **189**, 37-53.
- Chapman C.H., 1979. A new method for computing synthetic seismographs, *Geophys. J.R. astr. Soc.*, **64**, 321-372.
- Fuchs K. & Schulz K., 1976. Tunneling of low-frequency waves through the subcrustal lithosphere, *J. Geophys.*, **42**, 175-190.
- Gajewski D., Stangl R., Fuchs K. & Sandmeier K.J., A new constraint on the composition of the topmost continental mantle - anomalously different depth increases of P and S velocity, *Geophys. J. Int.*, **103**, 497-507.
- Grad M. & Luosto U., 1987. Seismic Models of the crust of the BALTIC shield along the SVEKA profile in Finland, *Annales Geophysicae*, **5B**, 639-650.
- Hirn A., 1977. Anisotropy in the continental upper mantle: possible evidence from explosion seismology, *Geophys. J. R. astr. Soc.*, **49**, 49-58.
- Jentsch M., 1979. Reinterpretation of a deep-seismic-sounding profile on the Ukrainian Shield, *J. Geophys.*, **45**, 355-372.
- Kaminski W., Bamford D., Faber S., Jacob B., Nunn K., Prodehl Co., 1976. A lithospheric seismic profile in Britain - II. A preliminary report on the recording of a local earthquake, *J. Geo-phys.*, **42**, 103-110.
- Kennett B.L.N., 1977, The inversion of long-range refraction profiles, *J. Geophys.*, **43**, 243-256.
- Kennett B.L.N., 1985. On regional S., *Bull. seism. Soc. Am.*, **75**, 1077-1085.
- Kennett B.L.N., 1989a. Lg wave propagation in heterogeneous media, *Bull. seism. Soc. Am.*, **79**, 860-872.
- Kennett B.L.N., 1989b. On the nature of regional seismic phases - I. Phase representations for Pn, Pg, Sn, Lg. *Geophys. J.R. astr. Soc.*, **98**, 447-456.
- Kennett B.L.N. & Engdahl E.R., 1991. Travel times for global earthquake location and phase association, *Geophys. J. Int.*, **105**,
- Kind R., 1974. Long range propagation of seismic energy in the lower lithosphere, *J. Geophys.*, **40**, 189-202.
- Luosto U., Lanne E., Korhonen H., Guterch A., Grad M., Materzok R. & Perchuc E., Deep structure of the Earth's crust on the SVEKA profile in central Finland, *Annales Geophysicae*, **2**, 559-570.
- Luosto U., Flueh E.R., Lund C.-E. & Working Group, 1989. The crustal structure along the POLAR profile from seismic refraction investigations, *Tectonophys.*, **162**, 51-85.
- Yegorkin, A. V. & Chernyshov, N.M., 1983. Peculiarities of mantle waves from long-range profiles, *J. Geophys.*, **54**, 30-34.

Prof. Thomas Ahrens
Seismological Lab, 252-21
Division of Geological & Planetary Sciences
California Institute of Technology
Pasadena, CA 91125

Prof. Keiiti Aki
Center for Earth Sciences
University of Southern California
University Park
Los Angeles, CA 90089-0741

Prof. Shelton Alexander
Geosciences Department
403 Deike Building
The Pennsylvania State University
University Park, PA 16802

Dr. Ralph Alewine, III
DARPA/NMRO
3701 North Fairfax Drive
Arlington, VA 22203-1714

Prof. Charles B. Archambeau
CIRES
University of Colorado
Boulder, CO 80309

Dr. Thomas C. Bache, Jr.
Science Applications Int'l Corp.
10260 Campus Point Drive
San Diego, CA 92121 (2 copies)

Prof. Muawia Barazangi
Institute for the Study of the Continent
Cornell University
Ithaca, NY 14853

Dr. Jeff Barker
Department of Geological Sciences
State University of New York
at Binghamton
Vestal, NY 13901

Dr. Douglas R. Baumgardt
ENSCO, Inc
5400 Port Royal Road
Springfield, VA 22151-2388

Dr. Susan Beck
Department of Geosciences
Building #77
University of Arizona
Tucson, AZ 85721

Dr. T.J. Bennett
S-CUBED
A Division of Maxwell Laboratories
11800 Sunrise Valley Drive, Suite 1450
Reston, VA 22091

Dr. Robert Blandford
AFTAC/TT, Center for Seismic Studies
1330 North 17th Street
Suite 1450
Arlington, VA 22209-2308

Dr. G.A. Bollinger
Department of Geological Sciences
Virginia Polytechnical Institute
21044 Derring Hall
Blacksburg, VA 24061

Dr. Stephen Bratt
Center for Seismic Studies
1300 North 17th Street
Suite 1450
Arlington, VA 22209-2308

Dr. Lawrence Burdick
Woodward-Clyde Consultants
566 El Dorado Street
Pasadena, CA 91109-3245

Dr. Robert Burrige
Schlumberger-Doll Research Center
Old Quarry Road
Ridgefield, CT 06877

Dr. Jerry Carter
Center for Seismic Studies
1300 North 17th Street
Suite 1450
Arlington, VA 22209-2308

Eric Chael
Division 9241
Sandia Laboratory
Albuquerque, NM 87185

Prof. Vernon F. Cormier
Department of Geology & Geophysics
U-45, Room 207
University of Connecticut
Storrs, CT 06268

Prof. Anton Dainty
Earth Resources Laboratory
Massachusetts Institute of Technology
42 Carleton Street
Cambridge, MA 02142

Prof. Steven Day
Department of Geological Sciences
San Diego State University
San Diego, CA 92182

Art Frankel
U.S. Geological Survey
922 National Center
Reston, VA 22092

Marvin Denny
U.S. Department of Energy
Office of Arms Control
Washington, DC 20585

Dr. Cliff Frolich
Institute of Geophysics
8701 North Mopac
Austin, TX 78759

Dr. Zoltan Der
ENSCO, Inc.
5400 Port Royal Road
Springfield, VA 22151-2388

Dr. Holly Given
IGPP, A-025
Scripps Institute of Oceanography
University of California, San Diego
La Jolla, CA 92093

Prof. Adam Dziewonski
Hoffman Laboratory, Harvard University
Dept. of Earth Atmos. & Planetary Sciences
20 Oxford Street
Cambridge, MA 02138

Dr. Jeffrey W. Given
SAIC
10260 Campus Point Drive
San Diego, CA 92121

Prof. John Ebel
Department of Geology & Geophysics
Boston College
Chestnut Hill, MA 02167

Dr. Dale Glover
Defense Intelligence Agency
ATTN: ODT-1B
Washington, DC 20301

Eric Fielding
SNEE Hall
INSTOC
Cornell University
Ithaca, NY 14853

Dr. Indra Gupta
Teledyne Geotech
314 Montgomery Street
Alexandria, VA 22314

Dr. Mark D. Fisk
Mission Research Corporation
735 State Street
P.O. Drawer 719
Santa Barbara, CA 93102

Dan N. Hagedorn
Pacific Northwest Laboratories
Battelle Boulevard
Richland, WA 99352

Prof Stanley Flatte
Applied Sciences Building
University of California, Santa Cruz
Santa Cruz, CA 95064

Dr. James Hannon
Lawrence Livermore National Laboratory
P.O. Box 808
L-205
Livermore, CA 94550

Dr. John Foley
NER-Geo Sciences
1100 Crown Colony Drive
Quincy, MA 02169

Dr. Roger Hansen
AFTAC/TTR
Patrick AFB, FL 32925

Prof. Donald Forsyth
Department of Geological Sciences
Brown University
Providence, RI 02912

Prof. David G. Harkrider
Seismological Laboratory
Division of Geological & Planetary Sciences
California Institute of Technology
Pasadena, CA 91125

Prof. Danny Harvey
CIRES
University of Colorado
Boulder, CO 80309

Prof. Donald V. Helmberger
Seismological Laboratory
Division of Geological & Planetary Sciences
California Institute of Technology
Pasadena, CA 91125

Prof. Eugene Herrin
Institute for the Study of Earth and Man
Geophysical Laboratory
Southern Methodist University
Dallas, TX 75275

Prof. Robert B. Herrmann
Department of Earth & Atmospheric Sciences
St. Louis University
St. Louis, MO 63156

Prof. Lane R. Johnson
Seismographic Station
University of California
Berkeley, CA 94720

Prof. Thomas H. Jordan
Department of Earth, Atmospheric &
Planetary Sciences
Massachusetts Institute of Technology
Cambridge, MA 02139

Prof. Alan Kafka
Department of Geology & Geophysics
Boston College
Chestnut Hill, MA 02167

Robert C. Kemerait
ENSCO, Inc.
445 Pineda Court
Melbourne, FL 32940

Dr. Max Koontz
U.S. Dept. of Energy/DP 5
Forrestal Building
1000 Independence Avenue
Washington, DC 20585

Dr. Richard LaCoss
MIT Lincoln Laboratory, M-200B
P.O. Box 73
Lexington, MA 02173-0073

Dr. Fred K. Lamb
University of Illinois at Urbana-Champaign
Department of Physics
1110 West Green Street
Urbana, IL 61801

Prof. Charles A. Langston
Geosciences Department
403 Deike Building
The Pennsylvania State University
University Park, PA 16802

Prof. Thorne Lay
Institute of Tectonics
Earth Science Board
University of California, Santa Cruz
Santa Cruz, CA 95064

Dr. William Leith
U.S. Geological Survey
Mail Stop 928
Reston, VA 22092

James F. Lewkowicz
Phillips Laboratory/GPEH
Hanscom AFB, MA 01731-5000

Mr. Alfred Lieberman
ACDA/VI-OA State Department Building
Room 5726
320-21st Street, NW
Washington, DC 20451

Prof. L. Timothy Long
School of Geophysical Sciences
Georgia Institute of Technology
Atlanta, GA 30332

Dr. Robert Masse
Denver Federal Building
Box 25046, Mail Stop 967
Denver, CO 80225

Dr. Randolph Martin, III
New England Research, Inc.
76 Olcott Drive
White River Junction, VT 05001

Dr. Gary McCartor
Department of Physics
Southern Methodist University
Dallas, TX 75275

Prof. Thomas V. McEvilly
Seismographic Station
University of California
Berkeley, CA 94720

Prof. Art McGarr
U.S. Geological Survey
Mail Stop 977
U.S. Geological Survey
Menlo Park, CA 94025

Dr. Keith L. McLaughlin
S-CUBED
A Division of Maxwell Laboratory
P.O. Box 1620
La Jolla, CA 92038-1620

Stephen Miller & Dr. Alexander Florence
SRI International
333 Ravenswood Avenue
Box AF 116
Menlo Park, CA 94025-3493

Prof. Bernard Minster
IGPP, A-025
Scripps Institute of Oceanography
University of California, San Diego
La Jolla, CA 92093

Prof. Brian J. Mitchell
Department of Earth & Atmospheric Sciences
St. Louis University
St. Louis, MO 63156

Mr. Jack Murphy
S-CUBED
A Division of Maxwell Laboratory
11800 Sunrise Valley Drive, Suite 1212
Reston, VA 22091 (2 Copies)

Dr. Keith K. Nakanishi
Lawrence Livermore National Laboratory
L-025
P.O. Box 808
Livermore, CA 94550

Dr. Carl Newton
Los Alamos National Laboratory
P.O. Box 1663
Mail Stop C335, Group ESS-3
Los Alamos, NM 87545

Dr. Bao Nguyen
AFTAC/TTR
Patrick AFB, FL 32925

Prof. John A. Orcutt
IGPP, A-025
Scripps Institute of Oceanography
University of California, San Diego
La Jolla, CA 92093

Prof. Jeffrey Park
Kline Geology Laboratory
P.O. Box 6666
New Haven, CT 06511-8130

Howard Patton
Lawrence Livermore National Laboratory
L-025
P.O. Box 808
Livermore, CA 94550

Dr. Frank Pilotte
HQ AFTAC/TT
Patrick AFB, FL 32925-6001

Dr. Jay J. Pulli
Radix Systems, Inc.
2 Taft Court, Suite 203
Rockville, MD 20850

Dr. Robert Reinke
ATTN: FCTVTD
Field Command
Defense Nuclear Agency
Kirtland AFB, NM 87115

Prof. Paul G. Richards
Lamont-Doherty Geological Observatory
of Columbia University
Palisades, NY 10964

Mr. Wilmer Rivers
Teledyne Geotech
314 Montgomery Street
Alexandria, VA 22314

Dr. George Rothe
HQ AFTAC/TTR
Patrick AFB, FL 32925-6001

Dr. Alan S. Ryall, Jr.
DARPA/NMRO
3701 North Fairfax Drive
Arlington, VA 22209-1714

Dr. Richard Sailor
TASC, Inc.
55 Walkers Brook Drive
Reading, MA 01867

Prof. Charles G. Sammis
Center for Earth Sciences
University of Southern California
University Park
Los Angeles, CA 90089-0741

Prof. Christopher H. Scholz
Lamont-Doherty Geological Observatory
of Columbia University
Palisades, CA 10964

Dr. Susan Schwartz
Institute of Tectonics
1156 High Street
Santa Cruz, CA 95064

Secretary of the Air Force
(SAFRD)
Washington, DC 20330

Office of the Secretary of Defense
DDR&E
Washington, DC 20330

Thomas J. Sereno, Jr.
Science Application Int'l Corp.
10260 Campus Point Drive
San Diego, CA 92121

Dr. Michael Shore
Defense Nuclear Agency/SPSS
6801 Telegraph Road
Alexandria, VA 22310

Dr. Matthew Sibol
Virginia Tech
Seismological Observatory
4044 Derring Hall
Blacksburg, VA 24061-0420

Prof. David G. Simpson
IRIS, Inc.
1616 North Fort Myer Drive
Suite 1400
Arlington, VA 22209

Donald L. Springer
Lawrence Livermore National Laboratory
L-025
P.O. Box 808
Livermore, CA 94550

Dr. Jeffrey Stevens
S-CUBED
A Division of Maxwell Laboratory
P.O. Box 1620
La Jolla, CA 92038-1620

Lt. Col. Jim Stobie
ATTN: AFOSR/NL
Bolling AFB
Washington, DC 20332-6448

Prof. Brian Stump
Institute for the Study of Earth & Man
Geophysical Laboratory
Southern Methodist University
Dallas, TX 75275

Prof. Jeremiah Sullivan
University of Illinois at Urbana-Champaign
Department of Physics
1110 West Green Street
Urbana, IL 61801

Prof. L. Sykes
Lamont-Doherty Geological Observatory
of Columbia University
Palisades, NY 10964

Dr. David Taylor
ENSCO, Inc.
445 Pineda Court
Melbourne, FL 32940

Dr. Steven R. Taylor
Los Alamos National Laboratory
P.O. Box 1663
Mail Stop C335
Los Alamos, NM 87545

Prof. Clifford Thurber
University of Wisconsin-Madison
Department of Geology & Geophysics
1215 West Dayton Street
Madison, WI 53706

Prof. M. Nafi Toksoz
Earth Resources Lab
Massachusetts Institute of Technology
42 Carleton Street
Cambridge, MA 02142

Dr. Larry Turnbull
CIA-OSWR/NED
Washington, DC 20505

DARPA/RMO/SECURITY OFFICE
3701 North Fairfax Drive
Arlington, VA 2203-1714

Dr. Gregory van der Vink
IRIS, Inc.
16116 North Fort Myer Drive
Suite 1440
Arlington, VA 22209

HQ DNA
ATTN: Technical Library
Washington, DC 20305

Dr. Karl Veith
EG&G
5211 Auth Road
Suite 240
Suitland, MD 20746

Defense Intelligence Agency
Directorate for Scientific & Technical Intelligence
ATTN: DTIB
Washington, DC 20340-6158

Prof. Terry C. Wallace
Department of Geosciences
Building #77
University of Arizona
Tucson, AZ 85721

Defense Technical Information Center
Cameron Station
Alexandria, VA 22314 (5 Copies)

Dr. Thomas Weaver
Los Alamos National Laboratory
P.O. Box 1663
Mail Stop C335
Los Alamos, NM 87545

TACTEC
Battelle Memorial Institute
505 King Avenue
Columbus, OH 43201 (Final Report)

Dr. William Wortman
Mission Research Corporation
8560 Cinderbed Road
Suite 700
Newington, VA 22122

Phillips Laboratory
ATTN: XPG
Hanscom AFB, MA 01731-5000

Prof. Francis T. Wu
Department of Geological Sciences
State University of New York
at Binghamton
Vestal, NY 13901

Phillips Laboratory
ATTN: GPE
Hanscom AFB, MA 01731-5000

AFTAC/CA
(STINFO)
Patrick AFB, FL 32925-6001

Dr. Michel Bouchon
I.R.I.G.M.-B.P. 68
38402 St. Martin D'Heres
Cedex, FRANCE

DAARPA/PM
3701 North Fairfax Drive
Arlington, VA 22203-1714

Dr. Michel Campillo
Observatoire de Grenoble
I.R.I.G.M.-B.P. 53
38041 Grenoble, FRANCE

DARPA/RMO/RETRIEVAL
3701 North Fairfax Drive
Arlington, VA 22203-1714

Dr. Kin Yip Chun
Geophysics Division
Physics Department
University of Toronto
Ontario, CANADA

Prof. Hans-Peter Harjes
Institute for Geophysics
Ruhr University/Bochum
P.O. Box 102148
4630 Bochum 1, GERMANY

Prof. Eystein Husebye
NTNF/NORSAR
P.O. Box 51
N-2007 Kjeller, NORWAY

David Jepsen
Acting Head, Nuclear Monitoring Section
Bureau of Mineral Resources
Geology and Geophysics
G.P.O. Box 378, Canberra, AUSTRALIA

Ms. Eva Johannisson
Senior Research Officer
National Defense Research Inst.
P.O. Box 27322
S-102 54 Stockholm, SWEDEN

Dr. Peter Marshall
Procurement Executive
Ministry of Defense
Blacknest, Brimpton
Reading FG7-FRS, UNITED KINGDOM

Dr. Bernard Massinon, Dr. Pierre Mechler
Societe Radiomana
27 rue Claude Bernard
75005 Paris, FRANCE (2 Copies)

Dr. Svein Mykkeltveit
NTNF/NORSAR
P.O. Box 51
N-2007 Kjeller, NORWAY (3 Copies)

Prof. Keith Priestley
University of Cambridge
Bullard Labs, Dept. of Earth Sciences
Madingley Rise, Madingley Road
Cambridge CB3 0EZ, ENGLAND

Dr. Jorg Schlittenhaardt
Federal Institute for Geosciences & Nat'l Res.
Postfach 510153
D-3000 Hannover 51, GERMANY

Dr. Johannes Schweitzer
Institute of Geophysics
Ruhr University/Bochum
P.O. Box 1102148
4360 Bochum 1, GERMANY